Global modeling study of potentially bioavailable iron input from shipboard aerosol sources to the ocean

Akinori Ito[1]

Received 2 April 2012; revised 27 September 2012; accepted 4 November 2012.

[1] Iron (Fe) is an essential element for phytoplankton. The majority of iron is transported from arid and semiarid regions to the open ocean, but it is mainly in an insoluble form. Since most aquatic organisms can take up iron only in the dissolved form, aerosol iron solubility is a key factor that can influence the air-sea CO_2 fluxes and thus climate. Field observations have shown relatively high iron solubility in aerosols influenced by combustion sources, but specific emissions sources and their contributions to deposition fluxes largely remain uncertain. Here a global chemical transport model was used to investigate the effect of aerosol emissions from ship plumes on iron solubility in particles from the combustion and dust sources. The model results reveal that the oil combustion from shipping mainly contributes to high iron solubility (>10%) at low iron loading (1–110 ng m^{-3}) observed over the high-latitude North Atlantic Ocean, rather than the other combustion sources from continental industrialized regions. Due to continuing growth in global shipping and no regulations regarding particles emissions over the open ocean, the input of potentially bioavailable iron from ship plumes is likely to increase during the next century. The model results suggest that deposition of soluble iron from ships in 2100 contributes 30–60% of the soluble iron deposition over the high-latitude North Atlantic and North Pacific.

Citation: Ito, A. (2013), Global modeling study of potentially bioavailable iron input from shipboard aerosol sources to the ocean, *Global Biogeochem. Cycles*, *27*, doi: 10.1029/2012GB004378.

1. Introduction

[2] Iron (Fe) scarcity has been shown to limit the biological primary productivity in high-nitrate, low-chlorophyll (HNLC) regions, such as the North Pacific, eastern equatorial Pacific, and the Southern Ocean [*Boyd and Ellwood*, 2010]. The present study focuses on shipboard aerosol sources that could enhance the aerosol iron solubility (i.e., the percentage of total aerosol iron that is soluble in water), which is a key uncertainty in our understanding of the global biogeochemical cycle of iron and climate. A multimodel study evaluated the projected changes (2080–2099, compared to 1870–1889) in marine productivity from four different coupled-carbon-climate models [*Steinacher et al*., 2010]. The projected marine productivity is highly sensitive to the input of iron from the atmosphere [*Mahowald*, 2011]. The ocean biogeochemical models typically assume iron solubility in the aerosols at 1–2%, but atmospheric observations have shown that iron in the aerosols can have a solubility ranging from 0.01 to 80% [*Mahowald et al*., 2009]. These results suggest that atmospheric models need to predict the large variability in iron solubility, instead of using a single value, to accurately predict the effects of changes in iron inputs on marine productivity and climate [*Mahowald*, 2011].

[3] High iron solubility (>10%) is often associated with low iron loadings (<100 ng m^{-3}) [*Sedwick et al*., 2007]. To explain this inverse relationship between iron solubility and iron loading, several hypotheses have been proposed, including source chemical composition, atmospheric processing, and aerosol size (i.e., larger surface area-to-volume ratio of smaller aerosol particles) [*Baker and Croot*, 2010]. *Chuang et al*. [2005] suggested that the emissions of soluble iron (SFe) from combustion sources can contribute to a significant fraction of SFe in the East Asian region, based on the measurements of SFe in aerosols at a regional sampling site (GOSAN) on the west end of Jeju Island, south of the Korean Peninsula. When the ratio (0.02) of SFe to black carbon (BC) observed at the GOSAN site was used in an atmospheric transport model, deposition of SFe from combustion sources contributed 40–100% of the SFe deposition over the HNLC regions (e.g., eastern equatorial Pacific and the Southern Ocean) [*Luo et al*., 2008]. The source chemical hypothesis states that the initial composition of the aerosol materials can be a critical control on the observed trends in iron solubility versus iron loading [*Sedwick et al*., 2007; *Sholkovitz et al*., 2009].

[4] The diesel engines on oceangoing vessels and oil boilers in heating and power plants produce fine particles that contain inorganic materials (e.g., S, V, Ni, Fe, Cr, and Na),

[1]Research Institute for Global Change, JAMSTEC, Yokohama, Kanagawa, Japan.

Corresponding author: A. Ito, Research Institute for Global Change, JAMSTEC, Yokohama, Kanagawa, 236–0001, Japan. (akinorii@jamstec.go.jp)

0886-6236/13/2012GB004378

BC, and particulate organic matter. The lowest-grade fuels (heavy fuel oils, residual fuel oils, crude oils, or bunker fuels) are typically used in the marine engines. *Siefert et al.* [1999] observed sporadic high iron solubility and fine vanadium fraction over the Arabian Sea, suggesting possible influences by the ship's plume. The aerosols influenced by air masses from North America or Europe have shown a large correlation between iron solubility and atmospheric loadings of vanadium and nickel, each of which are associated with emissions from the oil combustion [*Sholkovitz et al.*, 2009]. *Desboeufs et al.* [2005] reported higher value of iron solubility for oil fly ash (36%) than those for coal fly ash (0.2%) and urban dust (3.0%). A laboratory study indicates that oil combustion products yield much higher iron solubility (77–81%), compared to that of arid soils (<1%) [*Schroth et al.*, 2009]. A single-particle chemical analysis of iron-containing aerosols suggests that the ship emissions regionally change the chemical composition of aerosols during the Asian outflow season [*Furutani et al.*, 2011]. These field and laboratory studies might highlight the importance of highly soluble iron-containing aerosols emitted from the oil combustion on shipboard.

[5] Previous global model studies have demonstrated that the contributions of combustion aerosols, such as those from fossil fuel (FF) combustion and biomass burning (BB) to SFe deposition, are highly sensitive to uncertainties in iron solubility due to limited available observations [*Luo et al.*, 2008; *Ito*, 2012]. Since a significant fraction (45–75%) of the organic matter in BB aerosols is water soluble, water-soluble metal-organic compounds (e.g., $C_7H_6N_2O_4Fe$) can be emitted during BB [*Chang-Graham et al.*, 2011] and have the potential for long-range atmospheric transport and deposition to the open ocean [*Ito*, 2011]. When a high value of the SFe solubility observed for BB aerosols (18%) [*Bowie et al.*, 2009] was used in an atmospheric chemistry transport model, these combustion sources contributed 30–100% of the total supply of SFe to the equatorial and southern oceans downwind from open vegetation fires [*Ito*, 2012]. In the previous modeling studies, however, no distinction was made between the different sources of dissolved iron in the FF combustion aerosols, such as those from oil and coal combustion. The chemical and physical properties are different between oil and coal fly ash [*Desboeufs et al.*, 2005; *Sholkovitz et al.*, 2009]. Iron in oil fly ash is mainly present as ferric sulfate salt [*Schroth et al.*, 2009], which might be formed via high-temperature combustion (>800 °C) followed by a sulfuric acid condensation before filtration [*Sippula et al.*, 2009]. On the other hand, coal fly ash has a crust-like composition with a large amount of aluminosilicate glass, which might be formed via high-temperature combustion followed by a fast cooling process [*Chen et al.*, 2012]. It should be noted that atmospheric processing of mineral aerosols by inorganic and organic acids from anthropogenic and natural sources has been shown to increase the iron solubility of soils (initially <0.5%) up to about 10% [*Hand et al.*, 2004; *Meskhidze et al.*, 2005; *Ito and Feng*, 2010; *Luo and Gao*, 2010].

[6] Here a global chemical transport model was used to investigate the effect of aerosol particles emitted from the ship plumes on soluble iron input to the ocean, compared to those from the dust sources and the other combustion sources, such as those from coal combustion and BB. To assess model assumptions for iron dissolution, the calculated iron solubility was evaluated against a compilation of measurements from cruises over the oceans, mainly in the high-latitude Northern Hemisphere (NH). The model provides the first projection of SFe supply from shipping to the world's oceans in 2100, based on the Intergovernmental Panel on Climate Change (IPCC) emission scenario of Representative Concentration Pathway (RCP) 4.5 [*Thomson et al.*, 2011]. The RCP4.5 is a scenario that stabilizes radiative forcing at 4.5 $W m^{-2}$ in the year 2100 without ever exceeding that value.

2. Methods

2.1. Model Description

[7] The global chemical transport model used in this study is an aerosol chemistry version of the Integrated Massively Parallel Atmospheric Chemical Transport model [*Rotman et al.*, 2004; *Liu et al.*, 2005; *Feng and Penner*, 2007; *Ito and Feng*, 2010; *Ito*, 2011, 2012; *Ito et al.*, 2012]. The model simulates the emissions, chemistry, transport, and deposition of major aerosol species, including sulfate, nitrate, ammonium, fly ash (e.g., iron), BC, particulate organic matter, mineral dust and sea salt aerosols, and their precursor gases. The model is driven by assimilated meteorological fields from the Goddard Earth Observation System of the NASA Global Modeling and Assimilation Office (GMAO). Simulations have been performed at a horizontal resolution of 2.0°×2.5° with 42 vertical layers from 2001 to 2006.

[8] In our model, the SFe content in aerosols depends on source chemical composition [*Ito and Feng*, 2010; *Ito*, 2012]. The emission data sets for combustion-generated aerosols, such as those from FF combustion and BB (except oil combustion from ship) are taken from our emission inventory [*Ito and Penner*, 2005; *Ito et al.*, 2007; *Ito*, 2011]. Total ship emissions of particulate matter (PM), which include international shipping, domestic shipping, and fishing, are taken from an assessment of emission inventories in 2000 [*Eyring et al.*, 2010]. The upper and lower bound for total ship emissions of 1.4 Tg PM was 0.4–3.4 Tg PM [*Eyring et al.*, 2010]. To calculate 2001–2006 emissions, the 2000 emissions have been scaled with the changes in the total seaborne trade from *Fearnleys* [2007]. The ratio of total seaborne trade in 2006 to 2000 was 1.3 [*Fearnleys*, 2007]. The spatial allocation of anthropogenic emissions of FF use from each sector follows the grids generated for the IPCC Fifth Assessment (AR5) report [*Lamarque et al.*, 2010].

[9] The net emission factors of iron for each category of FF use have been calculated from the emission factors of PM [*Bond et al.*, 2004; *Ito and Penner*, 2005; *Eyring et al.*, 2010] and the iron content in aerosol particles [*Luo et al.*, 2008; *Ito and Feng*, 2010] (Tables 1 and 2). Here the emission factor for heavy fuel oil combustion from ships is compared with that from stationary sources (Table 3). The emission factor of iron for fine particles in g Fe/10^6g fuel, EF_{FineFe}, can be described by equation (1):

$$EF_{FineFe} = EF_{PM} \times F_{Fine} \times F_{Fe} \times F_{cont}, \quad (1)$$

where EF_{PM} is the bulk particulate emission factor in g/10^3g fuel, F_{Fine} is the fraction of the emissions with diameters smaller than 1 or 2.5 μm, F_{Fe} is the fraction of the iron content in fine particles, and F_{cont} is the fraction of fine particles that penetrates the control device. For combustion without

Table 1. Emission Factors of Iron in Fine Particles From FF Combustion

Fuel Category	Developed	Developing	Semideveloped
Coal Transformation			
Coke ovens	44	166	85
Blast furnaces	0.27	0.78	0.46
Briquettes	2.9	9.6	5.3
Rest of transformation	1.4	7.7	3.3
Coal Industry			
Iron and steel	6	48	18
Rest of industry	15	22	18
Coal residential	0.003	0.005	0.002
Oil Combustion			
Boiler	0.6	4.6	1.7
Ship	45	45	45
Incinerator	1.9	1.9	1.9

Units are g Fe/10^6 g fuel. The net emission factors have been calculated from the emission factors of fine PM [*Bond et al*., 2004; *Ito and Penner*, 2005; *Eyring et al*., 2010] and the iron content in fine particles [*Luo et al*., 2008; *Ito and Feng*, 2010].

Table 2. Emission Factors of Iron in Coarse Particles From FF Combustion

Fuel Category	Developed	Developing	Semideveloped
Coal Transformation			
Coke ovens	109	261	169
Blast furnaces	2.7	7.9	4.7
Rest of transformation	19	96	43
Coal Industry			
Iron and steel	281	781	468
Nonmetallic minerals	178	86	124
Rest of industry	178	86	124
Coal residential	0.25	0.51	0.36
Oil Combustion			
Boiler	1.4	10.7	3.9
Ship	14	14	14
Incinerator	15	15	15

Units are g Fe/10^6 g fuel. The net emission factors have been calculated from the emission factors of coarse PM [*Bond et al*., 2004; *Ito and Penner*, 2005; *Eyring et al*., 2010] and the iron content in coarse particles [*Luo et al*., 2008; *Ito and Feng*, 2010].

Table 3. Comparison of Emission Factors for Fine Particles From Heavy Fuel Oil Combustion

	EF_{PM}	F_{Fine}	F_{Fe}	F_{cont}	EF_{FineFe}
Ships	5.6	0.86	0.94%	1.0	45
Stationary sources	1.1	0.45	0.94%	0.13–1.0	0.6–4.6

EF_{PM} is the bulk particulate emission factor in g/10^3 g fuel. F_{Fine} is the fraction of the emissions in fine particles. F_{Fe} is the fraction of the iron content in fine particles. F_{cont} is the fraction of fine particles that penetrates the control device. EF_{FineFe} is the emission factor of iron for fine particles in g Fe/10^6 g fuel.

emission controls (e.g., shipping), F_{cont}=1.0. The emission factor of total PM for shipping from more recent assessment by *Eyring et al*. [2010] (5.6 g kg^{-1}) is significantly higher than that used by *Bond et al*. [2004] (1.8±1.5 g kg^{-1}). The fraction of the emissions in fine particles (e.g., 0.86 for shipping and 0.45 for stationary sources) is taken from *Bond et al*. [2004]. The arithmetic mean of the iron content for oil combustion aerosols used in this study (0.94% for fine particles and 1.8% for coarse particles) [*Mamuro et al*., 1979; *Mamane et al*., 1986; *Olmez et al*., 1988; *Hildemann et al*., 1991] is within the wide range of oil fly ash (0.2–4%) [*Sholkovitz et al*., 2009], but is smaller than the value in *Olmez et al*. [1988] used by *Luo et al*. [2008] (1.6% for fine particles and 3% for coarse particles). The resulting estimate of iron emission factor in fine particles from ships (45 g Fe/10^6 g fuel) is substantially larger than those from stationary sources (0.6–4.6 g Fe/10^6 g fuel), mainly because the vast majority of marine engines operate without effective reduction technologies [*Eyring et al*., 2010].

[10] Soluble component of iron from the combustion sources is readily released into solution in aerosols. In contrast, the emissions of dust are calculated on-line, based on the surface wind speed and soil wetness from the GMAO assimilated meteorological fields [*Ginoux et al*., 2001; *Ito et al*., 2012]. Furthermore, the iron solubility changes dynamically from that in the originally emitted dust aerosols (which is 0.45%) due to reactions with acidic species [*Ito and Feng*, 2010; *Ito*, 2012].

2.2. Sensitivity Experiments

[11] For the standard simulation (Experment 1), iron solubility in oil combustion is assumed at 79% [*Schroth et al*., 2009], while those in coal combustion and BB aerosols are at 11% [*Desboeufs et al*., 2005; *Chen et al*., 2012] and 18% [*Bowie et al*., 2009], respectively (Table 4). In addition to the Experiment 1 base case simulation, four sensitivity simulations have been conducted with different values of iron solubility for different combustion sources.

[12] A previous version of our model [*Ito et al*., 2012] uses iron solubility of 4% for all combustion sources (Experiment 2) [*Luo et al*., 2008], based on the measurements of SFe in aerosols at the GOSAN site [*Chuang et al*., 2005]. The observational site is located between the sources and remote conditions with a great gradient in aerosol concentration. *Chuang et al*. [2005] observed a good correlation between SFe and elemental carbon concentrations, but no correlation between elemental carbon and water-soluble potassium. Their results suggested that elemental carbon and soluble iron were coemitted as primary pollutants from the same sources, but BB was not a primary source.

[13] In our standard simulation, iron solubility in oil combustion is based on the solubility measurement of one fly ash from a power-plant sample in *Schroth et al*. [2009]. However, the value of 79% might be too high to represent a global value for iron in oil fly ash. In a third simulation (Experiment 3), the medium value for oil fly ash from *Desboeufs et al*. [2005] and *Schroth et al*. [2009] (36–79%) is examined.

Table 4. Summary of Iron Solubility Used in Sensitivity Simulations

	Oil From Ships (%)	Oil From Stationary Sources(%)	Coal (%)	Biomass (%)
Experiment 1	79	79	11	18
Experiment 2	4	4	4	4
Experiment 3	58	58	11	18
Experiment 4	79	79	22	18
Experiment 5	4	79	11	18

[14] In our standard simulation, iron solubility in coal combustion aserosol is obtained from the medium value for coal fly ash from *Desboeufs et al*. [2005] (0.2%) and *Chen et al*. [2012] (20–25%). Most of the iron in combustion aerosols comes from coal combustion in coarse particles [*Luo et al*., 2008]. The anthropogenic coal fly ash aerosol may represent a significant source of potentially bioavailable iron in the open ocean. In a fourth simulation, the effect of coal combustion sources on iron solubility in aerosols are examined by assuming high iron solubility (22%) from coal burning [*Chen et al*., 2012] (Experiment 4), while the experiment used the same iron solubility for others as in Experiment 1 (Table 4).

[15] In our standard simulation, the same iron solubility is used for oil combustion aerosols from shipping and stationary sources. It has been suggested that the oil combustion from continental industrialized regions may contribute to significant influences on the magnitude and spatial distribution of SFe input to the surface ocean [*Sedwick et al*., 2007]. The aerosols collected over the high-latitude North Atlantic are not only influenced by oil combustion sources from North America or Europe, but also by those from oceangoing vessels over the coastal regions and North Atlantic. In a fifth simulation, the effect of stationary sources on iron solubility in aerosols are examined by assuming lower iron solubility (4%) from shipping only (Experiment 5), while the experiment used the same iron solubility for others as in Experiment 1 (Table 4).

[16] In a future projection of soluble iron deposition changes, the anthropogenic emission changes in the primary sources of carbonaceous aerosols from 2000 to 2100 [*Thomson et al*., 2011] are used together with the standard solubility case for iron-containing aerosols (Experiment 1). The RCP4.5 scenario prescribes that pollution control levels increase over time in all countries as a function of income. Importantly, future scenarios demonstrate that significant technological improvements are needed to offset increased emissions from shipping due to the projected growth in seaborne trade, but particulate matter is not subject to international emission legislation over the open ocean [*Eyring et al*., 2010]. The increase of the shipping emissions from 2000 to 2005 (1.09) in RCP4.5 is smaller than that of total seaborne trade (1.25) [*Fearnleys*, 2007], while that from 2000 to 2050 (1.5) in RCP4.5 is in the middle of the possible range of future particle emissions according to four different technology scenarios and four different ship-traffic demand scenarios (0.9–2.1) [*Eyring et al*., 2010]. Thus, the projected estimates of emissions from shipping in RCP4.5 may be optimistic about environmental policy, although the projected increase of the shipping emissions in RCP4.5 is the highest among the four emission scenarios for IPCC AR5 (0.1–1.6). Keeping in mind that the future increase in emissions for shipboard aerosol sources may be conservative, the iron emissions are assumed to change linearly with the emissions of carbonaceous aerosols from RCP4.5. The resulting estimate of iron emission from shipping in 2100 (24 Fe Gg yr^{-1}) is a factor of 1.6 larger than the estimate in 2001 (16 Fe Gg yr^{-1}). The distribution of emissions from shipping may change due to growth in ship activity in Asian waters, emission control in coastal areas with heavy traffic, and decline in Arctic sea-ice extent [*Eyring et al*., 2010]. These changes need to be taken into account in future studies.

[17] In our approach, the effects of climate change, land-use change, and atmospheric composition change on natural sources, such as soil-derived dust and wild fires, are not taken into account. Thus, present-day estimates for mineral aerosols from arid and semiarid regions as well as for BB aerosols from boreal forest fires are used together with those for precursor gases of SO_2, NO_2, and NH_3. Note that future projections of dust deposition to the ocean are largely uncertain [*Mahowald et al*., 2009], due, in part, to uncertainty in the size distribution of mineral aerosols [*Kok*, 2011; *Ito et al*., 2012]. It is also noted that glacial dust sources are potentially important contributors of iron to the high-latitude oceans [*Schroth et al*., 2009; *Crusius et al*., 2011]. Moreover, further research is needed to improve our understanding of the processes that increase iron solubility in mineral particles for future projections.

2.3. Cruise-Based Observational Data

[18] To assess model assumptions for iron solubility, the calculated relationship between iron solubility and iron loading is evaluated against a compilation of measurements from cruise ships over the oceans (Figure 1). The daily average of model results was calculated from hourly output at the surface along the cruise tracks in order to compare the model with the compilation of ambient measurements from 2001 to 2006 [*Chen and Siefert*, 2004; *Baker et al*., 2006a, 2006b; *Buck et al*., 2006, 2010; *Sedwick et al*., 2007; *Aguilar-Islas et al*., 2010; *Hsu et al*., 2010; unpublished data of Baker and Powell in *Sholkovitz et al*., 2012]. Here the high-latitude North Atlantic Ocean (red squares in Figure 1) and the East China Sea (blue squares in Figure 1) are highlighted. The aerosol samples (indicated by red squares in Figure 1) were classified as air masses from the North Atlantic, North America, or Europe by *Chen and Siefert* [2004], *Baker*

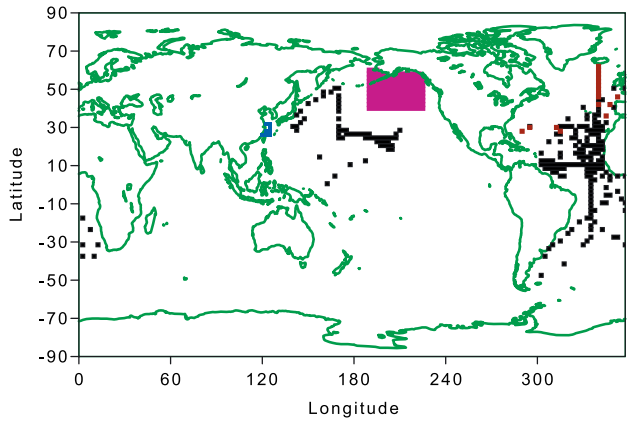

Figure 1. The locations of ship cruises from 2001 to 2006 are represented using square symbols in black and red over the Atlantic and Pacific oceans [*Chen and Siefert*, 2004; *Baker et al*., 2006a, 2006b; *Buck et al*., 2006, 2010; *Sedwick et al*., 2007; *Aguilar-Islas et al*., 2010; unpublished data of Baker and Powell in *Sholkovitz et al*., 2012] and in blue over the East China Sea [*Hsu et al*., 2010]. The aerosol samples classified as air masses from the North Atlantic, North America, or Europe are represented in red. The delimited area (purple box) is the HNLC region (40–60°N; 190–225°E) in the northeastern Pacific Ocean and is used to calculate monthly SFe deposition (Gg $month^{-1}$) in Figure 6 and Table 6.

et al. [2006a], *Sedwick et al*. [2007] and *Buck et al*. [2010]. A significant positive correlation between SFe and anthropogenic aerosols suggests that particles collected over the East China Sea were influenced by atmospheric chemical processing due to anthropogenic acids and mixing with combustion aerosols [*Hsu et al*., 2010].

3. Results and Discussion

3.1. SFe Emission

[19] The geographical distribution of SFe emissions are compared between different sources of oil combustion, coal combustion, BB, and dust (Figure 2). The majority of the emission from oil combustion occurs over the oceans within international sea routes in the NH (80%). Coal combustion sources are mostly located in China, India, Europe, and the northeastern United States, while BB sources are largely in the tropical regions. The dust sources are predominantly from North Africa, the Arabian Peninsula, East Asia, Australia, southern Africa, Chile, and Patagonia. The total emission of soluble iron in 2001 for the oil combustion aerosols from shipping (13 SFe Gg yr^{-1}) is much smaller than that for the dust (334 SFe Gg yr^{-1}) and other combustion aerosols (189 SFe Gg yr^{-1}) (Table 5). However, the majority of iron from coal combustion is in the coarse particle (88%), which is consistent with *Luo et al*. [2008]. Consequently, the emission of SFe in the fine particles for the oil combustion (9.5 SFe Gg yr^{-1}) is larger than that for the coal combustion (6.8 SFe Gg yr^{-1}).

Table 5. Estimates of SFe Emissions From Combustion Sources (SFe Gg yr^{-1})

Year	Oil Combustion (%)	Coal Combustion	BB
Fine Particles			
2001	9.5 (90)	6.8	25
2100	15 (98)	1.9	17
Coarse Particles			
2001	2.9 (70)	48	102
2100	4.5 (93)	13	71

The parentheses represent the percentage of ships to total oil combustion.

3.2. Aerosol Iron Solubility in Relation to Aerosol Sources and Iron Loadings

[20] The aerosol iron loadings from the model simulations are compared with measurements from 2001 to 2006 (Figure 3) [*Chen and Siefert*, 2004; *Baker et al*., 2006a, 2006b; *Buck et al*., 2006, 2010; *Sedwick et al*., 2007; *Aguilar-Islas et al*., 2010; *Hsu et al*., 2010; unpublished data of Baker and Powell in *Sholkovitz et al*., 2012]. The red circles represent the aerosol samples, which were collected over the high-latitude North Atlantic Ocean and were classified as air masses from the

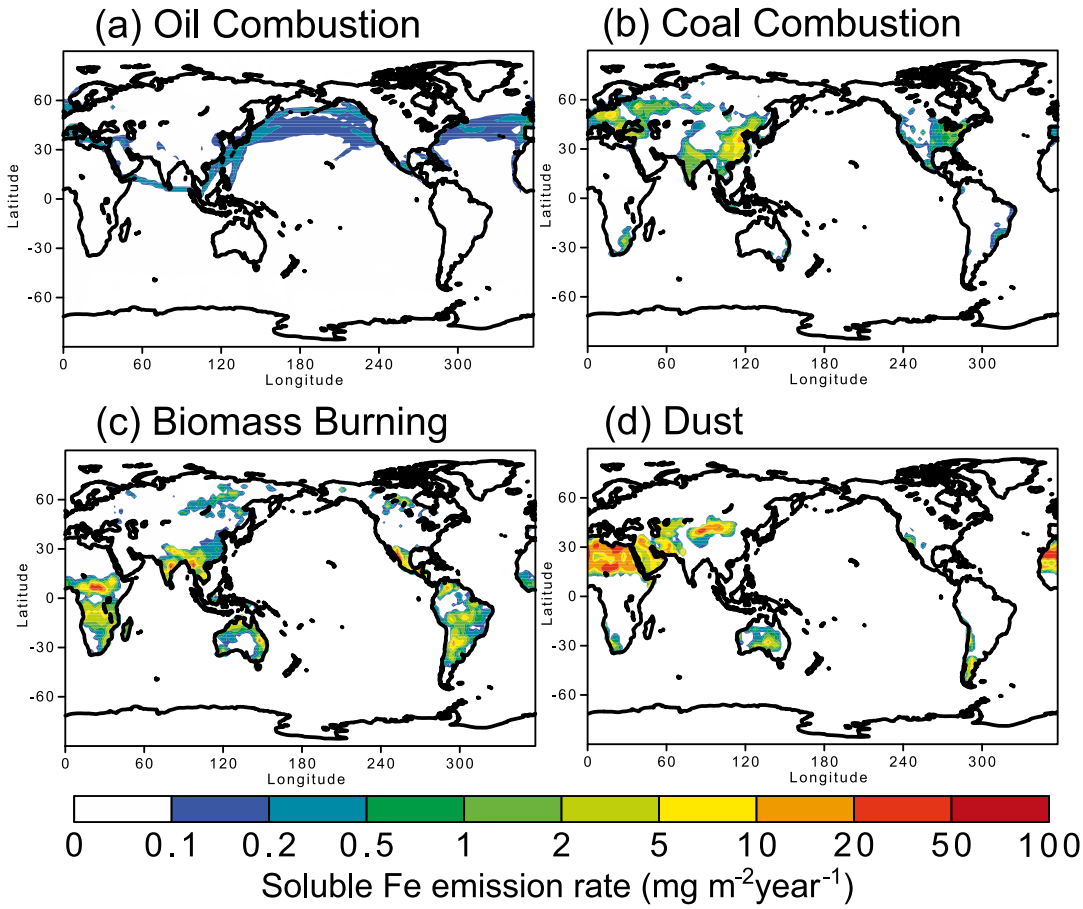

Figure 2. Annually averaged emission rates (mg m^{-2} $year^{-1}$) of SFe from (a) oil combustion, (b) coal combustion, (c) BB, and (d) dust in 2001. Contours are plotted for SFe emission rates above 0.1 mg m^{-2} $year^{-1}$.

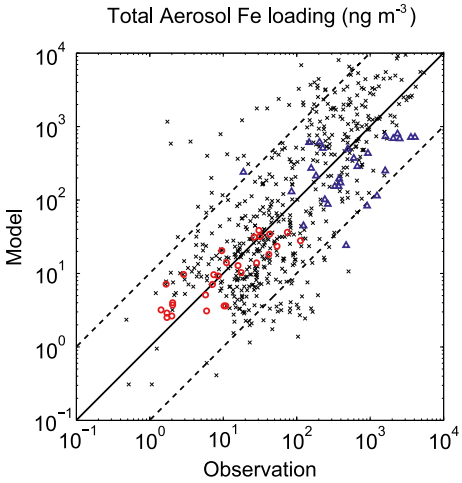

Figure 3. Comparison of simulated and observed aerosols for the total iron loadings (ng m^{-3}) over the Atlantic and Pacific oceans and the East China Sea. The total iron loadings are same for the experiments of Experiment 1, Experiment 2, Experiment 3, Experiment 4, and Experiment 5. The solid line represents a one-to-one correspondence. The dashed lines show deviations from the solid line by a factor of ±10. In comparison with the compilation of ambient measurements, the daily averages of model results were calculated from hourly output in the surface air along the cruise tracks. The aerosol samples classified as air masses from the North Atlantic, North America, or Europe are represented as red circles. The data collected over the East China Sea are represented as blue triangles.

North Atlantic, North America, or Europe. The high-latitude North Atlantic samples are characterized by extremely low-aerosol iron loadings (1–110 ng m^{-3}). The aerosol samples collected over the East China Sea are represented as blue triangles. The aerosol iron loading over the East China Sea (10–10^4 ng m^{-3}) is significantly larger than that over the high-latitude North Atlantic Ocean. Our model results have shown reasonable agreement of total iron loadings with observations over the wide range (1–10^4 ng m^{-3}) [*Ito et al.*, 2012].

[21] The aerosol iron solubility versus iron loading from the simulations (Experiment 1, Experiment 2, Experiment 3, Experiment 4, and Experiment 5) is shown in Figure 4, together with the observations (iron solubility <50%) [*Chen and Siefert*, 2004; *Baker et al.*, 2006a, 2006b; *Buck et al.*, 2006, 2010; *Sedwick et al.*, 2007; *Aguilar-Islas et al.*, 2010; *Hsu et al.*, 2010; unpublished data of Baker and Powell in *Sholkovitz et al.*, 2012]. The number of data points (Figure 4a) and the mean bias between the model results and observations are also presented for each experiment (Figures 4b–4f). The model results with highly soluble iron-containing aerosols from oil combustion are quite successful in simulating the hyperbolic relationship between iron solubility versus iron loading (Figure 4b), as opposed to those with lower iron solubility case (Figure 4c). The averaged iron solubility from this work (Experiment 1) over the high-latitude North Atlantic (red circles in Figure 4) is higher than that over the other locations (15±10% vs. 5±4%), which is consistent with the observations (16±11% vs. 6±8%), unlike our previous model results (Experiment 2) (4±1% vs. 4±2%) [*Ito et al.*, 2012]. The use of a conservative value (58%) for oil fly ash (Experiment 3) also improves the model measurement agreement (Figure 4d), compared to the lower iron solubility case (Experiment 2), but the mean bias (−4.1%) is larger than that using the high value of 79% (−1.2%). The iron solubility over the East China Sea is sensitive to that in coal fly ash. The model with higher iron solubility (22%) for coal combustion (Experiment 4) tends to overestimate sporadic high iron solubility (>10%) over the East China Sea (Figure 4e). Furthermore, if lower solubility (4%) for shipping, but higher solubility for stationary sources (79%), are used (Experiment 5), the model fails to reproduce the high iron solubility over the high-latitude North Atlantic (Figure 4f). These results may suggest that the combustion sources from continental industrialized regions are unlikely to contribute to high iron solubility at low loading over the open ocean.

[22] The SFe loadings from the model simulations (Experiment 1 and Experiment 2) are compared with measurements from 2001 to 2006 (Figure 5) [*Chen and Siefert*, 2004; *Baker et al.*, 2006a, 2006b; *Buck et al.*, 2006, 2010; *Sedwick et al.*, 2007; *Aguilar-Islas et al.*, 2010; *Hsu et al.*, 2010; unpublished data of Baker and Powell in *Sholkovitz et al.*, 2012]. The modeled SFe loadings (Experiment 1) result in better agreement with observations over the high-latitude North Atlantic (red circles) and the East China Sea (blue triangles). These results indicate that the source-dependent composition is the important factor controlling the sporadic high iron solubility (>10%). The SFe loading over the East China Sea (1–10^2 ng m^{-3}) is larger than those over the high-latitude North Atlantic (10^{-1}–10 ng m^{-3}), in contrast to the iron solubility (0.4–20% vs. 4–50%). These results may reflect the mixing of the oil combustion aerosols of higher iron solubility with other crust-like aerosols of lower iron solubility, such as dust and coal combustion.

3.3. Atmospheric SFe Input to Ocean Ecosystems

[23] The 6-year averaged monthly depositions of SFe from shipping only to the HNLC region in the northeastern Pacific (purple box in Figure 1) are compared with that from sum of the other combustion and dust (Figure 6a). The SFe depositions from Asian dust aerosols are generally larger in the spring. The total SFe depositions from all the sources (black line plus red line in Figure 6a) during summer (about 0.2 SFe Gg $month^{-1}$) are comparable to those without the shipping sources (black line in Figure 6a) during the Asian outflow season (0.2–0.4 SFe Gg $month^{-1}$). It is noteworthy that highly soluble iron-containing aerosols from shipping contribute to a substantial deposition of SFe (about 40%) in summer (Figure 6b) when the formation of a shallow and strong thermocline might lead to the buildup of soluble iron from ship emissions in the surface sea water.

[24] The spatial pattern of SFe deposition rate to the oceans from ship emissions in 2100 (Figure 7) mainly reflects their source locations, which are mainly distributed in the NH (Figure 2). The SFe deposition rate from ship emissions ranges from 4 to 10 (pg m^{-2} s^{-1}) in the the high-latitude North Atlantic, North Pacific, and the East China Sea (Figure 7a). The global emission of SFe for the oil combustion aerosols from shipping in 2100 (16 SFe Gg yr^{-1}) is much smaller than that for the dust (334 SFe Gg yr^{-1}) and other combustion aerosols (53 SFe Gg yr^{-1}) (Table 5). However, the model results suggest that the combustion source from ships in 2100 contributes to a significant deposition rate of

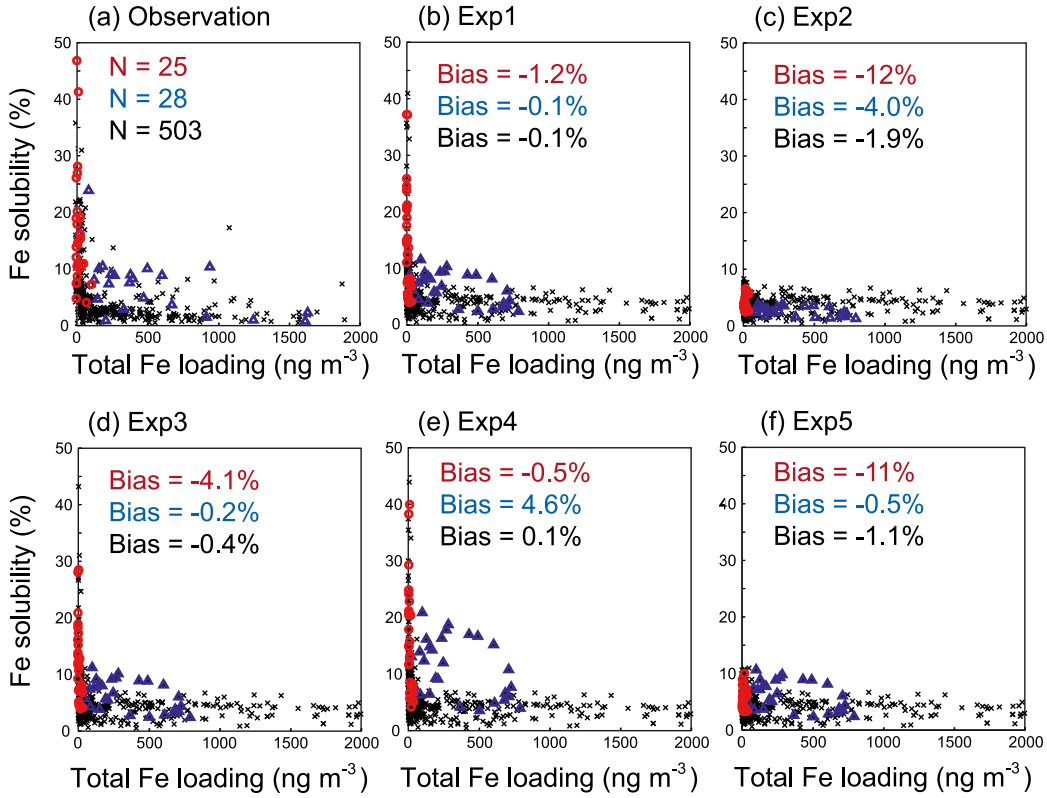

Figure 4. Comparison of (a) observed aerosols and simulated aerosols (b) Experiment 1, (c) Experiment 2, (d) Experiment 3, (e) Experiment 4, and (f) Experiment 5 for total iron loading ($ng m^{-3}$) vs. iron solubility (%) over the Atlantic and Pacific oceans and the East China Sea. The aerosol samples classified as air masses from the North Atlantic, North America, or Europe are represented as red circles. The data collected over the East China Sea are indicated as blue triangles. The number of data points (N) and the mean bias between the model results and observations are also shown.

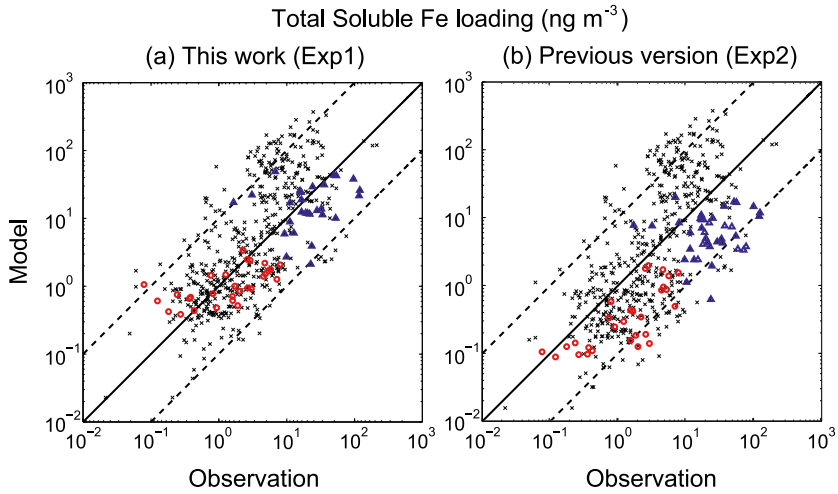

Figure 5. Comparison of simulated (a) Experiment 1 and (b) Experiment 2 and observed aerosols for soluble iron loading ($ng m^{-3}$) over the Atlantic and Pacific oceans and the East China Sea. The solid line represents a one-to-one correspondence. The dashed lines show deviations from the solid line by a factor of ±10. In comparison with the compilation of ambient measurements, the daily averages of model results were calculated from hourly output in the surface air along the cruise tracks. The aerosol samples classified as air masses from the North Atlantic, North America, or Europe are represented as red circles. The data collected over the East China Sea are indicated as blue triangles.

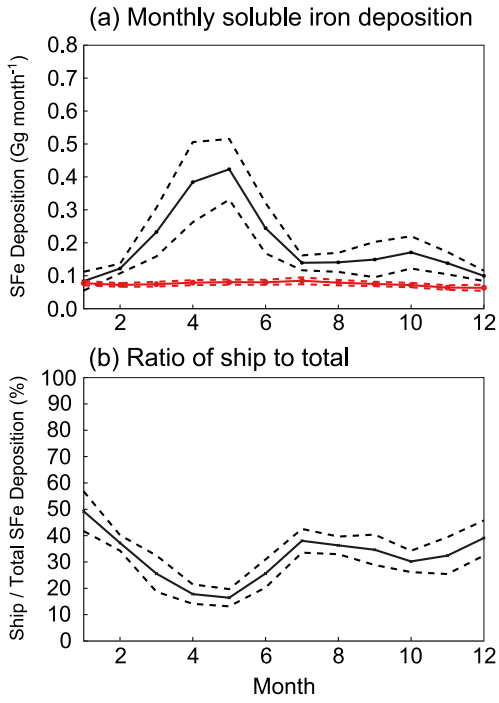

Figure 6. (a) Estimates of monthly SFe deposition (Gg month^{-1}) from shipboard combustion sources (red) and sum of the other combustion and dust sources (black) to HNLC regions in the northeastern Pacific Ocean (40–60°N; 190–225°E) for the present day. (b) Ratio (%) of the SFe deposition from shipping to that from the sum of all combustion and dust sources. The model results use the Experiment 1 value of 79% solubility for ship emission aerosol, as is summarized in Table 4. The dashed lines show the standard deviations of monthly averages during 2001–2006.

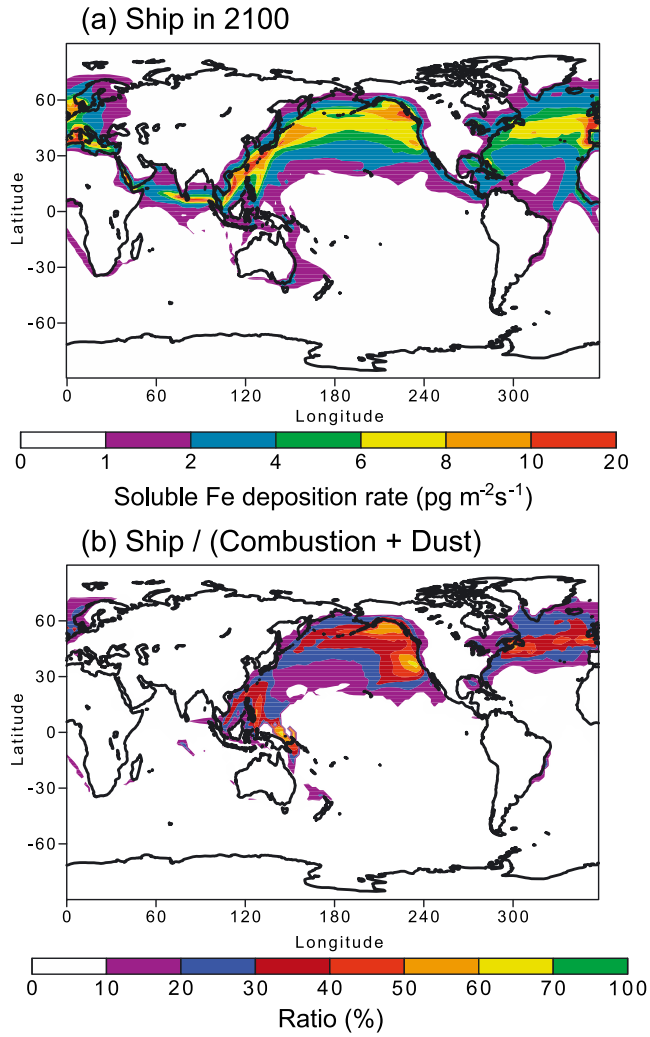

Figure 7. (a) Annually averaged SFe deposition rate (pg m^{-2} s^{-1}) from shipping in 2100. (b) Ratio (%) of the SFe deposition from shipping to that from the sum of combustion in 2100 and dust for the present day. Contours are plotted for SFe deposition rates from shipping above 1 pg m^{-2} s^{-1}. The results of the SFe deposition to HNLC regions in the northeastern Pacific Ocean (40–60°N; 190–225°E) are shown in Table 6.

SFe to the high-latitude North Atlantic and North Pacific (30–60%) (Figure 7b).

[25] In order to quantify the effects of the ship sources on total input into different regions of sea waters, the total depositions from different sources into the northeastern Pacific are compared with those into the East China Sea (Table 6). The model results indicate that the majority of iron is transported from arid and semiarid regions to the northeastern Pacific (99%) and the East China Sea (94%), but its iron solubility is low (0.7%). SFe form shipping is directly emitted over the ocean and thus significantly contributes to the northeastern Pacific (37%). The majority of iron from coal combustion is in the coarse particles (87%), which are preferentially removed from the atmosphere in our model treatment of deposition (i.e., faster deposition for larger particles). Consequently, SFe from the other combustion aerosols dominantly deposited to the East China Sea (41%), even though the SFe deposition rates from ships are comparable between the two different regions (6–10 pg m^{-2} s^{-1}) (Figure 7a).

4. Conclusions

[26] The chemical composition at emission is a key factor in reducing uncertainties in the prediction of a wide range of aerosol iron solubility. The association of oil combustion sources with high iron solubility (80%) improved the model results, compared to our previous assumption (4%). The model results suggest that highly soluble iron-containing aerosols from shipping may contribute about 40% of the SFe deposition into HNLC regions over the northeastern Pacific in summer, when the sporadic emission from Asian

Table 6. Depositions of Iron and SFe (Gg yr^{-1}) from Ship in 2100, Mineral Dust, and Other Combustion Sources to the Northeastern Pacific Ocean and the East China Sea

	Ship (%)	Dust (%)	Others (%)	Total
Northeastern Pacific Ocean				
Iron	1.6 (0.6)	290 (99)	1.2 (0.4)	293
SFe	1.3 (37)	2.0 (58)	0.2 (5.5)	3.5
East China Sea				
Iron	0.2 (0.4)	54 (94)	3.0 (5.3)	57
SFe	0.2 (18)	0.4 (41)	0.4 (41)	1.0

The parentheses represent the percentage of each source to total deposition.

dust is low. The results presented in this article could have important implications for the parameterization of iron dissolution and highlight the necessity to improve the source chemical composition. Further experiments to understand the character of the source of highly SFe in combustion aerosols are needed to represent the variability of iron solubility, because iron solubility is highly dependent on the physicochemical properties of the fly ash particles.

[27] The anthropogenic emission changes from 2000 to 2100 (RCP4.5) were applied to the global chemical transport model to examine the relative importance of shipping sources of SFe, compared with those from the other sources. The simulation results suggest that the combustion sources from ships in 2100 may contribute 30–60% of the SFe deposition in the high-latitude North Atlantic and North Pacific. The SFe form shipboard aerosol sources is directly emitted over the surface ocean and mostly supplied to the open ocean, such as the northeastern Pacific. In contrast, the majority of the crust-like aerosols, such as dust and coal fly ash, are deposited near the source regions, such as the East China Sea, because of faster removal for larger particles. Given the continuing growth in global shipping, it may be important to evaluate the role of iron from shipping in regulating marine biogeochemical processes.

[28] **Acknowledgments.** Support for this research was provided by the Program for Risk Information on Climate Change (MEXT). All of the numerical simulations were performed using the SGI Altix4700 at the JAMSTEC. The author would like to thank the reviewers for their constructive comments.

References

Aguilar-Islas, A. M., J. Wu, and R. Rember (2010), Dissolution of aerosol-derived iron in seawater: leach solution chemistry, aerosol type, and colloidal iron fraction, *Mar. Chem.*, *120*, 25–33, doi:10.1016/j.marchem.2009.01.011.

Baker, A. R., T. D. Jickells, M. Witt, and K. L. Linge (2006a), Trends in the solubility of iron, aluminium, manganese, and phosphorus in aerosol collected over the Atlantic Ocean, *Mar. Chem.*, *98*, 43–58, doi:10.1016/j.marchem.2005.06.004.

Baker A. R., M. French, and K. L. Linge (2006b), Trends in aerosol nutrient solubility along a west–east transect of the Saharan dust plume, *Geophys. Res. Lett.*, *33*, L07805, doi:10.1029/2005GL024764.

Baker, A. R., and P. L. Croot (2010), Atmospheric and marine controls on aerosol iron solubility in seawater, *Mar. Chem.*, *120*, 4–13, doi:10.1016/j.marchem.2008.09.003.

Bond, T. C., D. G. Streets, K. F. Yarber, S. M. Nelson, J. H. Woo, and Z. Klimont (2004), A technology-based global inventory of black and organic carbon emissions from combustion, *J. Geophys. Res.*, *109*, D14203, doi:10.1029/2003JD003697.

Bowie, A. R., D. Lannuzel, T. A. Remenyi, T. Wagener, P. J. Lam, P. W. Boyd, C. Guieu, A. T. Townsend, and T. W. Trull (2009), Biogeochemical iron budgets of the Southern Ocean south of Australia: Decoupling of iron and nutrient cycles in the subantarctic zone by the summertime supply, *Global Biogeochem. Cycles*, *23*, GB4034, doi:10.1029/2009GB003500.

Boyd, P. W. and M. J. Ellwood (2010), The biogeochemical cycle of iron in the ocean, *Nat. Geosci.*, *3*, 675–682, doi:10.1038/ngeo964.

Buck, C. S., W. M. Landing, J. A. Resing, and G. T. Lebon (2006), Aerosol iron and aluminum solubility in the northwest Pacific Ocean: Results from the 2002 IOC cruise, *Geochem. Geophys. Geosyst.*, *7*, Q04M07, doi:10.1029/2005GC000977.

Buck, C. S., W. M. Landing, and J. A. Resing (2010), Particle size and aerosol iron solubility: A high-resolution analysis of Atlantic aerosols, *Mar. Chem.*, *120*, 14–24, doi:10.1016/j.marchem.2008.11.002.

Chang-Graham, A. L., L. T. M. Profeta, T. J. Johnson, R. J. Yokelson, A. Laskin, and J. Laskin (2011), Case study of water-soluble metal containing organic constituents of biomass burning aerosol, *Environ. Sci. Technol.*, *45*, 1257, doi:10.1021/es103010j.

Chen, H., A. Laskin, J. Baltrusaitis, C. A. Gorski, M. M. Scherer, and V. H. Grassian (2012), Coal Fly Ash as a Source of Iron in Atmospheric Dust, *Environ. Sci. Technol.*, *46*, 2112–2120.

Chen, Y., and R. Siefert (2004), Seasonal and spatial distributions and dry deposition fluxes of atmospheric total and labile iron over the tropical and subtropical North Atlantic Ocean, *J. Geophys. Res.*, *109*, D09305, doi:10.1029/2003JD003958.

Chuang, P. Y., R. M. Duvall, M. M. Shafer, and J. J. Schauer (2005), The origin of water soluble particulate iron in the Asian atmospheric outflow, *Geophys. Res. Lett.*, *32*, L07813, doi:10.1029/2004GL021946.

Crusius, J., A. W. Schroth, S. Gassó, C. M. Moy, R. C. Levy, and M. Gatica (2011), Glacial flour dust storms in the Gulf of Alaska: Hydrologic and meteorological controls and their importance as a source of bioavailable iron, *Geophys. Res. Lett.*, *38*, L06602, doi:10.1029/2010GL046573.

Desboeufs, K. V., A. Sofikitis, R. Losno, J. L. Colin, and P. Ausset (2005), Dissolution and solubility of trace metals from natural and anthropogenic aerosol particulate matter, *Chemosphere*, *58*, 195–203, doi:10.1016/j.chemosphere.2004.02.025.

Eyring, V., I. S. A. Isaksen, T. Berntsen, W. J. Collins, J. J. Corbett, O. Endresen, R. G. Grainger, J. Moldanova, H. Schlager, and D. S. Stevenson (2010), Transport impacts on atmosphere and climate: Shipping, *Atmos. Environ.*, *44*, 4735–4771, doi:10.1016/j.atmosenv.2009.04.059.

Fearnleys (2007), *Fearnley's Review 2007*. The Tanker and Bulk Markets and Fleets, Oslo.

Feng, Y., and J. E. Penner (2007), Global modeling of nitrate and ammonium: Interaction of aerosols and tropospheric chemistry, *J. Geophys. Res.*, *112*, D01304, doi:10.1029/2005JD006404.

Furutani, H., J. Jung, K. Miura, A. Takami, S. Kato, Y. Kajii, and M. Uematsu (2011), Single-particle chemical characterization and source apportionment of iron-containing atmospheric aerosols in Asian outflow, *J. Geophys. Res.*, *116*, D18204, doi:10.1029/2011JD015867.

Ginoux, P., M. Chin, I. Tegen, J. M. Prospero, B. Holben, O. Dubovik, and S.-J. Lin (2001), Sources and distributions of dust aerosols simulated with the GOCART model, *J. Geophys. Res.*, *106*, 20,255–20,274, doi:10.1029/2000JD000053.

Hand, J. L., N. Mahowald, Y. Chen, R. Siefert, C. Luo, A. Subramaniam, and I. Fung (2004), Estimates of soluble iron from observations and a global mineral aerosol model: Biogeochemical implications, *J. Geophys. Res.*, *109*, D17205, doi:10.1029/2004JD004574.

Hildemann, L., G. Markowski, and G. Cass, (1991), Chemical composition of emissions from urban sources of fine organic aerosol, *Environ. Sci. Technol.*, *25*, 744–759, doi:10.1021/es00016a021.

Hsu, S.-C., G. T. F. Wong, G.-C. Gong, F.-K. Shiah, Y.-T. Huang, S.-J. Kao, F. Tsai, S.-C. Lung, F.-J. Lin, I.-I. Lin, C.-C. Hung, and C.-M. Tseng (2010), Sources, solubility, and dry deposition of aerosol trace elements over the East China Sea, *Mar. Chem.*, *120*, 116–127, doi:10.1016/j.marchem.2008.10.003.

Ito, A., and J. E. Penner (2005), Historical emissions of carbonaceous aerosols from biomass and fossil fuel burning for the period 1870–2000, *Global Biogeochem. Cycles*, *19*, GB2028, doi:10.1029/2004GB002374.

Ito, A., A. Ito, and H. Akimoto (2007), Seasonal and interannual variations in CO and BC emissions from open biomass burning in Southern Africa during 1998–2005, *Global Biogeochem. Cycles*, *21*, GB2011, doi:10.1029/2006GB002848.

Ito, A. and Y. Feng (2010), Role of dust alkalinity in acid mobilization of iron, *Atmos. Chem. Phys.*, *10*, 9237–9250, doi:10.5194/acp-10-9237-2010.

Ito, A. (2011), Mega fire emissions in Siberia: Potential supply of bioavailable iron from forests to the ocean, *Biogeosciences*, *8*, 1679–1697, doi:10.5194/bg-8-1679-2011.

Ito, A. (2012), Contrasting the effect of iron mobilization on soluble iron deposition to the ocean in the Northern and Southern Hemispheres, *J. Meteorol. Soc. Japan*, *90A*, 167–188, doi:10.2151/jmsj.2012-A09.

Ito, A., J. F. Kok, Y. Feng, and J. E. Penner (2012), Does a theoretical estimation of the dust size distribution at emission suggest more bioavailable iron deposition?, *Geophys. Res. Lett.*, *39*, L05807, doi:10.1029/2011GL050455.

Kok, J. F. (2011), A scaling theory for the size distribution of emitted dust aerosols suggests climate models underestimate the size of the global dust cycle, *Proc. Natl. Acad. Sci. U. S. A.*, *108*(3), 1016–1021, doi:10.1073/pnas.1014798108.

Lamarque, J.-F. T. C. Bond, V. Eyring, C. Granier, A. Heil, Z. Klimont, D. Lee, C. Liousse, A. Mieville, B. Owen, et al., (2010), Historical (1850–2000) gridded anthropogenic and biomass burning emissions of reactive gases and aerosols: Methodology and application, *Atmos. Chem. Phys.*, *10*, 7017–7039, doi:10.5194/acp-10-7017-2010.

Liu, X., J. E. Penner, and M. Herzog (2005), Global modeling of aerosol dynamics: Model description, evaluation, and interactions between sulfate and non-sulfate aerosols, *J. Geophys. Res.*, *110*, D18206, doi:10.1029/2004JD005674.

Luo, C., N. Mahowald, T. Bond, P. Y. Chuang, P. Artaxo, R. Siefert, Y. Chen, and J. Schauer (2008), Combustion iron distribution and

deposition, *Global Biogeochem. Cycles*, *22*, GB1012, doi:10.1029/2007GB002964.

Luo, C., and Y. Gao (2010), Aeolian iron mobilisation by dust-acid interactions and their implications for soluble iron deposition to the ocean: a test involving potential anthropogenic organic acidic species, *Environ. Chem.*, *7*, 153–161, doi:10.1071/EN09116.

Mahowald, N. M., S. Engelstaedter, C. Luo, A. Sealy, P. Artaxo, C. Benitez-Nelson, S. Bonnet, Y. Chen, P. Y. Chuang, D. D. Cohen, et al. (2009), Atmospheric iron deposition: Global distribution, variability, and human perturbations, *Annu. Rev. Mar. Sci.*, *1*, 245–278, doi:10.1146/annurev.marine.010908.163727.

Mahowald, N. (2011), Aerosol indirect effect on biogeochemical cycles and climate, *Science*, *334*, 794–796, doi:10.1126/science.1207374.

Mamane, Y., J. Miller, and T. Dzubay (1986), Characterization of individual fly ash particles emitted from coal- and oil-fired power plants, *Atmos. Environ.*, *20*, 2125–2135, doi:10.1016/0004-6981(86)90306-9.

Mamuro, T., A. Mizohata, and T. Kubota (1979), Elemental composition of suspended particles released from various boilers, *J. Jpn. Soc. Air Pollut.*, *14*, 296–303, (in Japanese).

Meskhidze, N., W. L. Chameides, and A. Nenes (2005), Dust and pollution: A recipe for enhanced ocean fertilization?, *J. Geophys. Res.*, *110*, D03301, doi:10.1029/2004JD005082.

Olmez, I., A. Sheffield, G. Gordon, J. Houck, L. Pritchett, J. Cooper, T. G. Dzubay, and R. Bennett (1988), Compositions of particles from selected sources in Philadelphia for receptor modeling applications, *J. Air Pollut. Control Assoc.*, *38*, 1392–1402, doi:10.1080/08940630.1988.10466479.

Rotman, D. A., C. S. Atherton, D. J. Bergmann, P. J. Cameron-Smith, C. C. Chuang, P. S. Connell, J. E. Dignon, A. Franz, K. E. Grant, D. E. Kinnison, et al. (2004), IMPACT, the LLNL 3-D global atmospheric chemical transport model for the combined troposphere and stratosphere: Model description and analysis of ozone and other trace gases, *J. Geophys. Res.*, *109*, D04303, doi:10.1029/2002JD003155.

Schroth, A. W., J. Crusius, E. R. Sholkovitz, and B. C. Bostick (2009), Iron solubility driven by speciation in dust sources to the ocean. *Nat. Geosci.*, *2*, 337–340, doi:10.1038/ngeo501.

Sedwick, P. N., E. R. Sholkovitz, and T. M. Church (2007), Impact of anthropogenic combustion emissions on the fractional solubility of aerosol iron: Evidence from the Sargasso Sea, *Geochem. Geophys. Geosyst.*, *8*, Q10Q06, doi:10.1029/2007GC001586.

Sholkovitz, E. R., P. N. Sedwick, and T. M. Church (2009), Influence of anthropogenic combustion emissions on the deposition of soluble aerosol iron to the ocean: Empirical estimates for island sites in the North Atlantic, *Geochim. Cosmochim. Acta*, *73*, 3981–4003, doi:10.1016/j.gca.2009.04.029.

Sholkovitz, E. R., P. N. Sedwick, T. M. Church, A. R. Baker, and C. F. Powell (2012), Fractional solubility of aerosol iron: Synthesis of a global-scale data set, *Geochim. Cosmochim. Acta*, *89*, 173–189, doi:10.1016/j.gca.2012.04.022.

Siefert, R. L., A. M. Johansen, and M. R. Hoffmann (1999), Chemical characterization of ambient aerosol collected during the southwest monsoon and intermonsoon seasons over the Arabian Sea: Labile-Fe(II) and other trace metals, *J. Geophys. Res.*, *104D*, 3511–3526, doi:10.1029/1998JD100067.

Sippula, O., J. Hokkinen, H. Puustinen, P. Yli-Pirilä, and J. Jokiniemi (2009), Comparison of particle emissions from small heavy fuel oil and wood-fired boilers, *Atmos. Environ.*, *43*, 4855–4864, doi:10.1016/j.atmosenv.2009.07.022.

Steinacher, M., F. Joos, T. L. Frlicher, L. Bopp, P. Cadule, V. Cocco, S. C. Doney, M. Gehlen, K. Lindsay, J. K. Moore, B. Schneider, and J. Segschneider (2010), Projected 21st century decrease in marine productivity: A multi-model analysis, *Biogeosciences*, *7*, 979–1005, doi:10.5194/bg-7-979-2010.

Thomson A. M., K. V. Calvin, S. J. Smith, G. P. Kyle, A. C. Volke, P. L. Patel, S. Delgado Arias, B. Bond-Lamberty, M. A. Wise, L. E. Clarke, et al. (2011), RCP4.5: a pathway for stabilization of radiative forcing by 2100, *Clim. Change*, *109*, 77–94, doi:10.1007/s10584-011-0151-4.